

and the fracture-promoting dislocations would move closer to the crack tip (21). Additional energy dissipation by dislocation motion is insignificant compared with crack-tip shielding at these low temperatures. Low-temperature fracture toughness increases with predeformation; thus other processes must be invoked. The only reasonable explanation is that the preexisting dislocations in the highly stressed vicinity of the crack tip act as sources for dislocations, which provide more efficient shielding.

At intermediate temperatures, the beneficial effect of the predeformation vanishes and the fracture toughness of the predeformed specimens is lower than that of the reference specimens. This is attributed to the increased yield strength and lower dislocation mobility produced by work hardening. The reduced dislocation mobility will not only decrease the fracture toughness but must also be expected to shift the BDTT to higher temperatures. Similar behavior is also found in NiAl single crystals (5). These observations strongly indicate that the BDT is controlled by dislocation mobility.

At low temperatures, dislocation nucleation is the limiting process because of the scarcity of active sources. When the temperature is sufficiently high to activate a large number of sources, or the number of active sources is increased by predeformation, dislocation mobility assumes control of the nucleation rate, and the fracture toughness becomes rate dependent. Such a loading rate dependence of the fracture toughness of tungsten is found in room temperature experiments but not at liquid nitrogen temperature. It is evident that any model for the BDT must necessarily include dislocation mobility and cannot be based exclusively on dislocation nucleation.

In the whole temperature regime of the present investigation, plasticity in tungsten is believed to be controlled by the mobility of the screw dislocations [for example, see (22)]. However, the activation energy for the glide of these dislocations is $Q_{\text{screw}} = 2 \text{ eV}$ (23, 24), whereas the activation energy for the BDT $Q_{\text{BDT}} = 0.2 \text{ eV}$ is much closer to the activation energy for the glide of nonscrew (edge) dislocations, $Q_{\text{edge}} = 0.2 \text{ to } 0.5 \text{ eV}$ (23, 25). Consequently, development of a plastic zone at the crack tip cannot be limited by the same mechanisms as bulk plasticity. A possible mechanism to lower the high activation barrier for screw dislocation motion could involve the high-stress region around the crack tip. If a dislocation—either one that is generated at the crack tip or a preexisting one—moves in the “singular” stress field along the crack tip, it will generate dislocation segments of nonscrew character parallel to the crack tip, which are highly mobile and must be expected to provide highly efficient shielding. However, the detailed mechanisms for the different crystallographic orientations of the crack remain to be clarified.

The results clearly show that the fracture toughness in the semibrittle fracture regime below the BDTT is strongly dependent on the availability and activity of dislocation sources. However, it becomes evident that, in materials other than dislocation-free silicon, the BDT itself is not controlled by the availability of sources but must be interpreted as a thermally activated process controlled by the mobility of dislocations.

References and Notes

- C. St. John, *Philos. Mag.* **32**, 1193 (1975).
- M. Brede and P. Haasen, *Acta Metall.* **36**, 2003 (1988).
- S. G. Roberts, A. S. Booth, P. B. Hirsch, *Mater. Sci. Eng.* **A176**, 91 (1994).
- H. Huang and W. W. Gerberich, *Acta Metall. Mater.* **42**, 639 (1994).
- F. Ebrahimi and S. Shrivastava, *Acta Mater.* **46**, 1493 (1998).
- J. R. Rice and R. Thomson, *Philos. Mag. A* **29**, 73 (1974).
- M. Khantha, D. Pope, V. Vitek, *Phys. Rev. Lett.* **73**, 684 (1994).
- P. B. Hirsch, S. G. Roberts, J. Samuels, *Proc. R. Soc. London Ser. A* **421**, 25 (1989).
- S. G. Roberts, in *Computer Simulations in Materials Science*, series E: *Applied Sciences*, vol. 308, H. O. Kirchner, L. P. Kubin, V. Pontikis, Eds. (Kluwer, Dordrecht, Netherlands, 1996), pp. 409–433.
- A. Hartmaier and P. Gumbsch, *Phys. Status Solidi B* **202**, R1 (1997).
- G. Michot, M. A. L. de Oliveira, A. George, *Mater. Sci. Eng.* **A176**, 99 (1994).
- J. Riedle, P. Gumbsch, H. F. Fischmeister, V. G. Lebovsky, V. N. Semenov, *Mater. Lett.* **20**, 311 (1994).
- The variability in the stress intensity rate mainly stems from variations in the length of the precrack.
- J. Riedle, thesis, Universität Stuttgart, Stuttgart (1995).
- J. Riedle, P. Gumbsch, H. F. Fischmeister, *Phys. Rev. Lett.* **76**, 3594 (1996).
- S. Kohlhoff, P. Gumbsch, H. F. Fischmeister, *Philos. Mag. A* **64**, 851 (1991).
- L. Berlec, *J. Appl. Phys.* **33**, 197 (1962).
- Y. Tamura, T. Fujii, Y. Ohba, *Trans. Inst. Met.* **14(5)**, 173 (1972).
- B. Devincere and S. G. Roberts, *Acta Mater.* **44**, 2891 (1996).
- J. Samuels and S. G. Roberts, *Proc. R. Soc. London Ser. A* **421**, 1 (1989).
- S. J. Zhou and R. Thomson, *J. Mater. Res.* **6**, 1763 (1991).
- A. S. Argon and S. R. Maloof, *Acta Metall.* **14**, 1449 (1966).
- U. Ziebart, thesis, Universität Stuttgart, Stuttgart (1986).
- D. Brunner, personal communication.
- H. W. Schadler, *Acta Metall.* **12**, 861 (1964).
- J.R. thanks S. Roberts for helpful discussions and hospitality at the University of Oxford, where part of this work was conducted. J.R. gratefully acknowledges partial financial support from Deutscher Akademischer Austauschdienst. A.H. acknowledges financial support from Deutsche Forschungsgemeinschaft (contract GU 367/1).

22 July 1998; accepted 8 October 1998

A Tough, Thermally Conductive Silicon Carbide Composite with High Strength up to 1600°C in Air

Toshihiro Ishikawa,* Shinji Kajii, Kenji Matsunaga, Toshihiko Hogami, Yasuhiko Kohtoku, Toshio Nagasawa

A sintered silicon carbide fiber-bonded ceramic, which consists of a highly ordered, close-packed structure of very fine hexagonal columnar fibers with a thin interfacial carbon layer between fibers, was synthesized by hot-pressing plied sheets of an amorphous silicon-aluminum-carbon-oxygen fiber prepared from an organosilicon polymer. The interior of the fiber element was composed of sintered β -silicon carbide crystal without an obvious second phase at the grain boundary and triple points. This material showed high strength (over 600 megapascals in longitudinal direction), fibrous fracture behavior, excellent high-temperature properties (up to 1600°C in air), and high thermal conductivity (even at temperatures over 1000°C).

Silicon carbide fiber-reinforced ceramic matrix composites (SiC-CMCs) are being developed as a candidate for toughened thermostructural materials (1). However, at present, no SiC-CMCs can withstand actual long use at high

temperatures (>1500°C) in air, because of the problems of heat resistance or oxidation resistance or both of the fiber and interphase (2, 3). Moreover, under load, cracks in the matrix caused by creep failure of the fiber also accelerate fatal oxidation of the composites (4). We developed a type of toughened SiC-based material containing perfectly close-packed, very fine hexagonal columnar fibers that consist of a sintered structure of β -SiC crystals. At the interface between the hexagonal columnar fibers,

Ube Research Laboratory, Corporate Research and Development, Ube Industries Limited, 1978-5 Kogushii, Ube City, Yamaguchi 755, Japan,

*To whom correspondence should be addressed. E-mail: 24613u@ube-ind.co.jp

a very thin interfacial carbon layer uniformly exists, which results in a fibrous fracture behavior. This material has a very high fiber volume fraction (~100%) and showed excellent oxidation resistance even at 1600°C in air and maintained the initial high strength up to such high temperatures. Furthermore, this material (sintered SiC fiber-bonded ceramic) showed relatively high thermal conductivity even at high temperatures (>1000°C), which would allow its use in the fabrication of high-temperature heat exchanger components.

An amorphous Si-Al-C-O fiber, which is the starting material of the sintered SiC fiber-bonded ceramic, was synthesized from polyaluminocarbosilane, which was prepared by the reaction of polycarbosilane (-SiH(CH₃)-CH₂)_n with aluminum(III) acetylacetonate. The reaction of polycarbosilane with aluminum(III) acetylacetonate proceeded at 300°C in a nitrogen atmosphere through the condensation reaction of Si-H bonds in polycarbosilane and the ligands of aluminum(III) acetylacetonate accompanied by the evolution of acetylacetone

(5). The molecular weight then increased because of the cross-linking reaction in the formation of the Si-Al-Si bond. Polyaluminocarbosilane was melt-spun at 220°C, and then the spun fiber was cured in air at 153°C. The cured fiber was continuously fired in inert gas up to 1350°C to obtain an amorphous Si-Al-C-O fiber with diameters of about 10 μm (87% between 8 and 12 μm). This fiber contained a nonstoichiometric amount of excess carbon and oxygen (about 11 weight %). Unidirectional sheets with thicknesses of about 100 μm were prepared with the Si-Al-C-O fiber. Laminated materials, prepared with the unidirectional sheets, were hot-pressed at 1800°C and 50 MPa to obtain the sintered SiC fiber-bonded ceramic mainly composed of β-SiC crystal (Fig. 1).

During hot-pressing, amorphous Si-Al-C-O fiber was converted into a sintered SiC fiber by way of a decomposition, which released CO gas, and a sintering process accompanied by a morphological change from a round columnar shape to a hexagonal columnar shape. In this sintering process, aluminum in the fiber has to be controlled under 1 weight %. Such a sintered SiC fiber element (with <1 weight % Al) showed a densified structure and transcrystalline fracture behav-

ior. The production process of the sintered SiC fiber-bonded ceramic is shown in Fig. 2.

The sintered SiC fiber-bonded ceramic showed a perfectly close-packed structure of the hexagonal columnar fibers with a very thin interfacial carbon layer (Fig. 3A). The interior of the fiber element was composed of sintered β-SiC crystal without an obvious second phase at the grain boundary and triple points (Fig. 3B). Energy-dispersive x-ray (EDX) spectra taken at these places did not indicate the presence of aluminum within the detectability limit (~0.5 weight %) for the EDX system used. Because of the existence of the very thin interfacial carbon layer, the sintered SiC fiber-bonded ceramic exhibited a fibrous fracture behavior and a large amount of fiber pull-out could be observed (Fig. 3C). Accordingly, the sintered SiC fiber-bonded ceramic showed nonlinear fracture behavior and relatively high fracture energy (1200 J/m²) compared with monolithic ceramics (for example, 80 J/m² for silicon nitride) (Fig. 3D). This is closely related to the high fiber volume fraction and the existence of a strictly controlled interphase. The interfacial carbon layer has a turbostratic layered structure oriented parallel to the fiber surface, as can be seen from a high-resolution transmission electron micrograph of the carbon layer (Fig. 3E).

The sintered SiC fiber-bonded ceramic showed excellent high-temperature properties compared with ordinary SiC-CMCs. The result of a four-point bending test of the sintered SiC fiber-bonded ceramic up to high temperatures is shown in Fig. 4A, along with the result for an ordinary SiC-CMC with a representative SiC fiber, Hi-Nicalon. The sintered SiC fiber-bonded ceramic retained its initial strength (for a unidirectional specimen, greater than 600 MPa) up to 1600°C, whereas the Hi-Nicalon SiC/SiC showed a definite decrease in strength at tem-

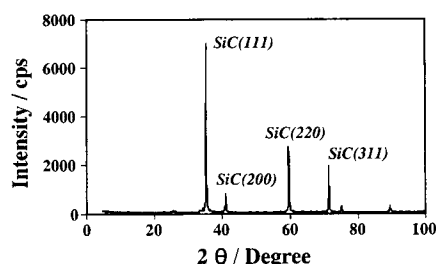


Fig. 1. X-ray diffraction pattern of the sintered SiC fiber-bonded ceramic. The sintered SiC fiber-bonded ceramic was pulverized, and the x-ray diffraction pattern of the powder was recorded with a Rigaku x-ray diffractometer with Cu K α radiation with a nickel filter.

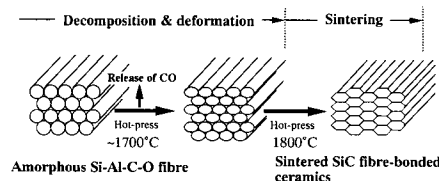


Fig. 2. Schematic of the production process for the sintered SiC fiber-bonded ceramic. The fiber is Si₁C_{1.5}O_{0.4}Al_{0.014}. The right panel shows the close-packed structure of the fiber with the interfacial carbon layer.

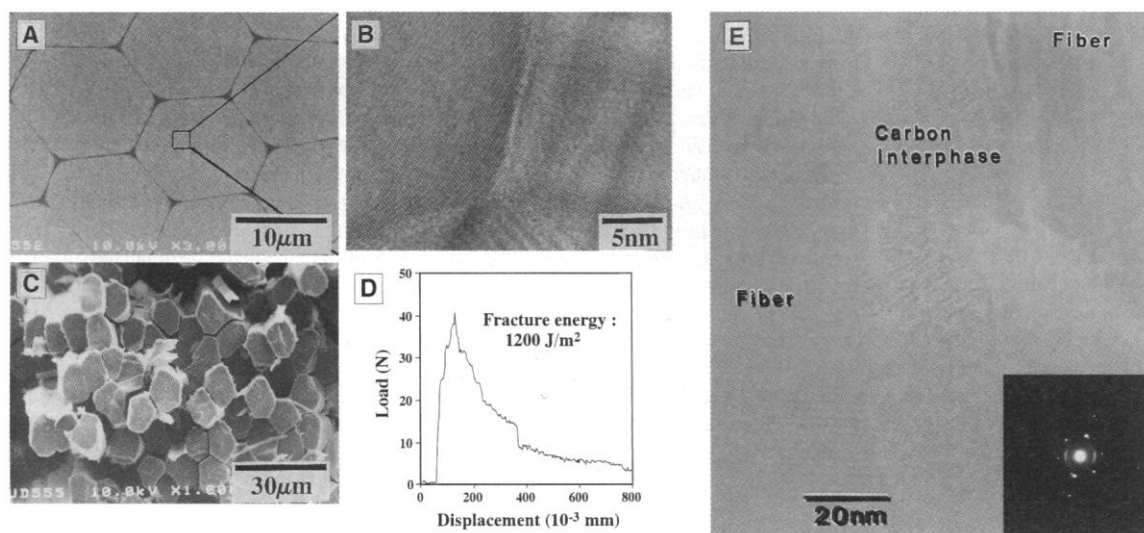


Fig. 3. (A) A scanning electron microscope (SEM) image of the cross section of the sintered SiC fiber-bonded ceramic. The box in (A) is enlarged in (B). (B) A transmission electron microscope (TEM) image near the SiC grain boundary in the fiber element of the sintered SiC fiber-bonded ceramic. (C) The fracture surface of the sintered SiC fiber-bonded ceramic. (D) The load-displacement curve of the sintered SiC fiber-bonded ceramic in fracture energy test by chevron notched beam method at room temperature. The fracture energy test was performed with a cross-plyed, notched specimen with dimensions of about 4 mm by 3 mm by 40 mm. (E) A high-resolution TEM image of the interfacial carbon layer of the sintered SiC fiber-bonded ceramic. The SEM image and the TEM images were obtained with a Hitachi S-5000 operated at 20 kV and JEOL 4000EX operated at 3000 kV, respectively.

iron notched beam method at room temperature. The fracture energy test was performed with a cross-plyed, notched specimen with dimensions of about 4 mm by 3 mm by 40 mm. (E) A high-resolution TEM image of the interfacial carbon layer of the sintered SiC fiber-bonded ceramic. The SEM image and the TEM images were obtained with a Hitachi S-5000 operated at 20 kV and JEOL 4000EX operated at 3000 kV, respectively.

peratures above 1200°C (3). Other types of SiC/SiC composites also show the same behavior as the Hi-Nicalon SiC/SiC (4, 6). In general, the high-temperature properties of conventional SiC-CMCs are closely related to the high-temperature strength of the reinforcing fiber. The strength of Hi-Nicalon gradually decreases with an increase of measuring temperature, even in inert atmosphere; at 1500°C, the strength is about 43% of its low-temperature strength (7). Accordingly, it has been concluded that the above reduction in the strength of the Hi-Nicalon SiC/SiC is due to the change in the fiber property at high temperatures. However, the sintered SiC fiber, which consists of the same composition and interior structure as the sintered SiC fiber-bonded ceramic, is very stable up to 2000°C (8). Moreover, the sintered SiC fiber shows negligible stress relaxation up to higher temperatures compared with other representative SiC fibers. On the basis of these findings, we attribute the high-temperature strength of the sintered SiC fiber-bonded ceramic to the high-temperature properties of the fiber element.

Researchers have been developing SiC-CMCs to obtain an oxidation-resistant, tough thermostructural material. In general, a SiC-based material easily forms a protective oxide layer on its surface at high temperatures in air, leading to the well-known excellent oxidation resistance. The formation of the protective oxide layer proceeds in air according to the following reaction:

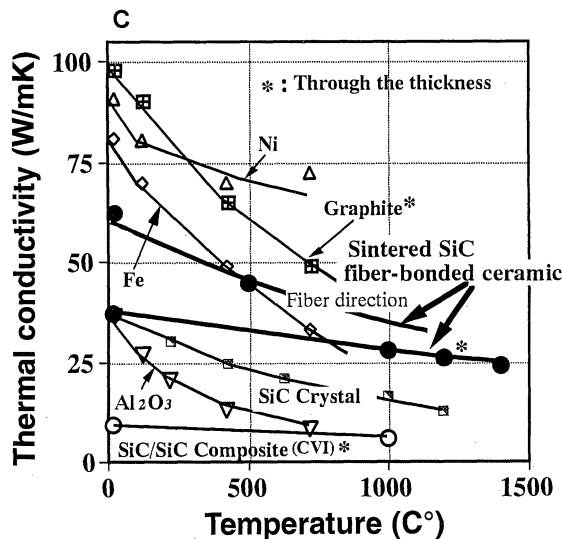
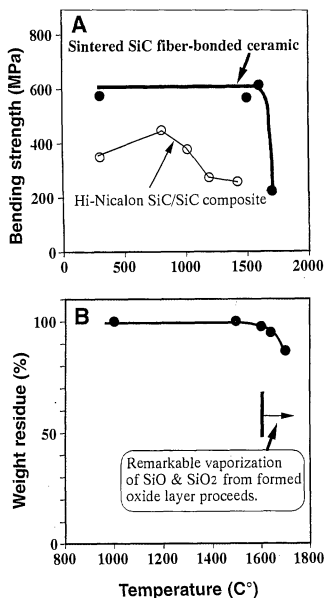
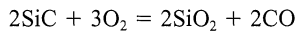


Fig. 4. (A) The strength of the sintered SiC fiber-bonded ceramic in a four-point bending test at various temperatures up to 1700°C. The SiC fiber-bonded ceramic is unidirectional. The Hi-Nicalon SiC/SiC composite is two-directional and has a three-point bending strength. (B) The weight changes of the sintered SiC fiber-bonded ceramic after heat treatment up to 1700°C in air for 10 hours. (C) Thermal conductivity of the sintered SiC fiber-bonded ceramic in the direction through the thickness and the fiber direction along with other materials including representative SiC/SiC composite (CVI). The thermal conductivity K was calculated as $K = WCD$, where W is the thermal diffusivity, C is the specific heat, and D is the density. The thermal diffusivity and specific heat were measured by a laser flash method.

In this reaction, the oxygen diffusion through the oxide layer is the rate-determining step. However, at temperatures above 1600°C in air, considerable vaporization of SiO or SiO₂ from the formed oxide layer begins to occur, so that a weight loss of the SiC-based material becomes conspicuous under the above conditions. Accordingly, as long as non-coated SiC-based material is used in air, the upper limit of temperature is at around 1600°C. The sintered SiC fiber-bonded ceramic, which showed no change even at 1800°C in argon, also showed no marked weight loss up to 1600°C in air (Fig. 4B), a temperature at which this material still retains its initial strength. From these findings, the sintered SiC fiber-bonded ceramic is found to be furnished with sufficient heat resistance even in air. To aid in the understanding of the oxidation behavior, we show a hypothesis concerning the structural changes of the sintered SiC fiber-bonded ceramic during oxidation at around 1600°C in air in Fig. 5.

The sintered SiC fiber-bonded ceramic has potential for use in heat exchangers because of its relatively high thermal conductivity at temperatures above 1000°C. Figure 4C shows the thermal conductivity of the sintered SiC fiber-bonded ceramic in the direction through the thickness and the fiber direction along with other materials including representative SiC/SiC composite (CVI).

In general, the thermal conductivity of ceramics with strong covalent bonds is caused mainly by the transmission of phonons (lattice vibration). According to this theory (9), the

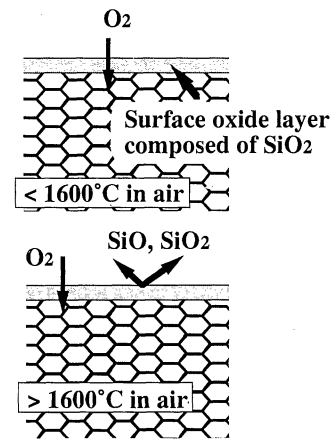


Fig. 5. A hypothesis concerning the structural changes of the sintered SiC fiber-bonded ceramic during oxidation at high temperatures at around 1600°C in air.

desirable conditions for high thermal conductivity are as follows: (i) small mass of constituent atoms, (ii) strong bonding strength between the constituent atoms, (iii) short distance between neighboring atoms, (iv) simple crystalline structure, and (v) high symmetry in lattice vibrations. Fundamentally, although the SiC crystal satisfies the above conditions, in the case of polycrystalline ceramics like the present sintered SiC fiber-bonded ceramic, an ordered structure at the grain boundary is important for obtaining high thermal conductivity. As mentioned above, in the fiber element of the fiber-bonded ceramic, many SiC crystals of 0.1 to 0.4 μm in diameter are directly in contact with other similar crystals without any obvious intercrystalline phase (Fig. 3B). Furthermore, the fiber-bonded ceramic showed almost void-less structure (porosity of less than 1 volume %) and very high fiber volume fraction (~100%). This structure accounts for the very high thermal conductivity of the sintered SiC fiber-bonded ceramic compared with other representative SiC-CMCs. For example, the thermal conductivity of Nicalon SiC/SiC (CVI) with a pyrolytic carbon interface is about 7 W/mK (1).

References

1. D. W. Richerson, *Mater. Eng. Composite Eng. Handb.* **11**, 983 (1997).
2. I. J. Davies, T. Ishikawa, N. Suzuki, M. Shibuya, T. Hirokawa, in *Proceedings of the 5th Japan International SAMPE Symposium* (Japan Chapter of SAMPE, Yokohama, 1997), pp. 1627-1632.
3. M. Takeda et al., *Ceram. Eng. Sci. Proc.* **18**, 779 (1997).
4. G. N. Morscher, *ibid.*, p. 737.
5. T. Yamamura, T. Ishikawa, M. Shibuya, Japanese Patent 1699835 (1992).
6. K. Ifflander and G. C. Gualco, *Ceram. Eng. Sci. Proc.* **18**, 625 (1997).
7. M. Tanaka et al., *ibid.* **14**, 540 (1993).
8. T. Ishikawa, Y. Kohtoku, K. Kumagawa, T. Yamamura, T. Nagasawa, *Nature* **391**, 773 (1998).
9. W. D. Kingery, H. K. Brown, D. R. Uhlman, *Introduction to Ceramics* (Wiley, New York, ed. 2, 1976).

5 June 1998; accepted 11 August 1998